Exact projection-operator formalism for highly correlated systems: Mean-field results for the CuO_2 lattice

A. J. Fedro
Department of Physics, Northern Illinois University, De Kalb, Illinois 60115
and Materials Science Division, Argonne National Laboratory, Argonne, Illinois 60439

Yu Zhou
Materials Science Division, Argonne National Laboratory, Argonne, Illinois 60439

T. C. Leung and B. N. Harmon
Ames Laboratory and Department of Physics, Iowa State University, Ames, Iowa 50011

S. K. Sinha
Corporate Research, Exxon Research & Engineering Co., Annandale, New Jersey 08801
(Received 6 February 1992)

We present an exact formulation of the single-particle Green's functions for the two-dimensional three-band Hubbard model of the CuO_2 lattice based on a projection-operator formalism of Mori. The model is general and incorporates the various known local-density-approximation (LDA) interaction parameters. In this paper we present only the mean-field results. The inclusion of self-energy effects will be presented elsewhere. Already, in the mean-field approximation, we find that properties such as hole occupations and magnetic moments compare remarkably well with those from quantum Monte Carlo (MC) calculations. The densities of states are also calculated for various hole dopings, again using the parameters from the LDA calculations. Finally the detailed effect of hopping between different O p orbitals, are also presented.

I. INTRODUCTION

The two-dimensional (2D) single-band Hubbard Hamiltonian[1] has been widely studied as a model for the high-T_c superconductors. Various theoretical techniques have been used to solve for its dynamics, including the exact diagonalization of small clusters,[2] quantum Monte Carlo (MC) simulations,[3] and various mean-field (MF) treatments.[4-8] However, not all electronic interactions existing in the CuO_2 plane can be easily incorporated into the single-band framework. Therefore, to gain a better understanding of the effects caused by the interactions between the Cu and O system, as well as the hopping between O p orbitals, it is necessary to study a more realistic model. In this paper we concentrate on the CuO_2 lattice which is formulated in terms of the three-band Hubbard model.

In the three-band Hubbard model,[9] each unit cell contains one Cu $d_{x^2-y^2}$ orbital and its two neighboring O p_x and p_y orbitals. The hybridizations between near-neighbor Cu and O atoms as well as that between near-neighbor O atoms are considered. The on-site Coulomb repulsions between any two holes in the same Cu d and O p states with opposite spins are also taken into account. Finally the near-neighbor intersite repulsion between the Cu and O atoms is also included. The resulting model Hamiltonian is written explicitly in Sec. II. This model has been extensively studied using quantum Monte Carlo techniques[10,11] and various mean-field formalisms.[12,13] However, because of the large number of interactions involved, it is common to ignore certain energy parameters in MC calculations, and complicated coupled equations have to be solved self-consistently in MF approximations.

Previously, we presented a Mori-projection-operator-based mean-field (POMF) calculation of the single-band Hubbard model[14] which yielded a systematic improvement over the Hubbard-I approximation and our results compared well with that of MC calculations and that of a particular form of slave-boson theory[7,8] (SBMF). An important advantage of the POMF formulation from the SBMF is that one does not separate the spin and charge degrees of freedom of the hole, which results in fewer coupled equations to be solved. This allows us to apply the POMF formalism to the multiband Hubbard model straightforwardly without much additional computational effort. As a test of the method, the hole occupation numbers on Cu and O sites as well as the magnetic moments have been calculated for some model parameters, and remarkable agreement with available MC results are obtained. The effect of the hybridization between two neighboring O atoms, designated by hopping energy t_{pp}, has also been studied. Here there are no MC results available. We find that t_{pp} suppresses the hole number and magnetic moment on Cu sites as expected. This will be discussed in detail in Sec. III. We have also calculated the Cu and O hole density of states (DOS) for various band fillings and for both antiferromagnetic (AF) and paramagnetic states, using the energy parameters obtained from local-density-approximation (LDA) calculations. We find that our DOS are distinctly different from

that in the Hubbard-I approximation, but resembles that obtained from the SBMF theory.

The paper is organized as follows: The formalism of the POMF theory is outlined in Sec. II and the detailed derivation is given in the Appendix. Section III contains the calculations and results for various electronic properties. The conclusions are presented in Sec. IV.

II. PROJECTION-OPERATOR FORMALISM

In this paper we present a projection operator method for determining the needed Green's functions. We are interested in the general Hamiltonian used in the theory of the 2D CuO_2 lattice which can be written in hole notation as follows:

$$\begin{aligned} H=&\varepsilon_d\sum_{j,\sigma}n_{j,\sigma}+U_{dd}\sum_j n_{j,+}n_{j,-}+\varepsilon_p\sum_{j,\lambda,\sigma}n_{j+\lambda/2,\sigma}+U_{pp}\sum_{j,\lambda}n_{j+\lambda/2,+}n_{j+\lambda/2,-}\\ &+U_{dp}\sum_{j,\alpha,\lambda,\sigma,\sigma'}n_{j,\sigma}n_{j+\alpha\lambda/2,\sigma'}-t_{dp}\sum_{j,\alpha,\sigma}[d^\dagger_{j\sigma}(p_{j+\alpha x/2,\sigma}-p_{j+\alpha y/2,\sigma})+\text{H.c.}]\\ &+t_{pp}\sum_{j,\sigma}[(p^\dagger_{j+x/2,\sigma}-p^\dagger_{j-x/2,\sigma})(p_{j+y/2,\sigma}-p_{j-y/2,\sigma})+\text{H.c.}]\ , \end{aligned} \tag{1}$$

where $\lambda=x,y$ and $\alpha=\pm$. Here the Cu d-hole operator for site j and spin σ is given by $d_{j\sigma}$ with the corresponding number operator $n_{j\sigma}=d^\dagger_{j\sigma}d_{j\sigma}$. The oxygen p-hole operators surrounding the jth Cu site are defined by $p_{j+\alpha\lambda/2,\sigma}$ with the corresponding number operators given by

$$n_{j+\alpha\lambda/2,\sigma}=p^\dagger_{j+\alpha\lambda/2,\sigma}p_{j+\alpha\lambda/2,\sigma}\ .$$

ε_d and ε_p are the on-site Cu and O energies, U_{dd} and U_{pp} are the corresponding on-site Coulomb repulsions, and U_{dp} is the near-neighbor Cu-O repulsion. t_{dp} is the near-neighbor Cu-O hopping matrix element and t_{pp} the O-O near-neighbor hopping matrix element. The orbital sign convention is such both t_{dp} and $t_{pp}>0$. The space lattice is defined to be that of the Cu's, i.e., a 2D square lattice of spacing a. The four surrounding oxygens are then at a distance $a/2$ from the central Cu atom. The LDA numbers for the parameters are given by[15]

$$\begin{aligned} &U_{dd}=10.5\text{ eV},\quad U_{pp}=4.0\text{ eV},\quad U_{dp}=1.2\text{ eV}\ ,\\ &t_{dp}=1.3\text{ eV},\quad t_{pp}=0.65\text{ eV},\quad \varepsilon\equiv\varepsilon_p-\varepsilon_d=3.6\text{ eV}\ . \end{aligned} \tag{2}$$

In this paper we will focus on comparisons to the available MC results as well as to other MF calculations where U_{dp} is generally set to zero. If $U_{dp}=0$, the multiband Hamiltonian in Eq. (1) has the general form

$$\begin{aligned} H=&\sum_{j,\nu,\sigma}\varepsilon_\nu n_{j\nu\sigma}+\sum_{j,\nu}U_{\nu\nu}n_{j\nu,+}n_{j\nu,-}\\ &+\sum_{j,j',\nu,\nu',\sigma}t_{j,\nu;j',\nu'}c^\dagger_{j\nu\sigma}c_{j'\nu'\sigma}\ , \end{aligned} \tag{3}$$

where j denotes the unit-cell position, and ν denotes the atoms in the unit cell. In this framework one can easily incorporate possible AF order. The hopping matrix elements are real and satisfy $t_{j\nu;j'\nu'}=t_{j'\nu';j\nu}$ with $t_{j\nu;j\nu}=0$. The site number operators are defined by $n_{j\nu\sigma}=c^\dagger_{j\nu\sigma}c_{j\nu\sigma}$. ε_ν are the single level energies and $U_{\nu\nu}$ the on-site repulsions. We now separate the pure Fermi excitation operators $c_{j\nu\sigma}$ into two operators $f^\alpha_{j\nu\sigma}$ (as done in the original work of Hubbard), with $\alpha=\pm$ as follows:

$$f^\alpha_{j\nu\sigma}=n^\alpha_{j\nu,-\sigma}c_{j\nu\sigma},\quad c_{j\nu\sigma}=\sum_\alpha f^\alpha_{j\nu\sigma}\ , \tag{4a}$$

etc., where we define

$$n^\alpha_{j\nu-\sigma}=\begin{cases}n_{j\nu-\sigma}, & \alpha=+\ ,\\ 1-n_{j\nu-\sigma}, & \alpha=-\ .\end{cases} \tag{4b}$$

Then the needed retarded Green's functions $G^{\alpha\alpha'}_{j\nu;j'\nu'\sigma}(t)$ are formed as follows:

$$G^{\alpha\alpha'}_{j\nu;j'\nu'\sigma}(t)=-i\langle[f^\alpha_{j\nu\sigma}(t),f^{\alpha'\dagger}_{j'\nu'\sigma}]_+\rangle\ ,\quad t\ge0\ , \tag{5}$$

where $f^\alpha_{j\nu\sigma}(t)$ are the ordinary Heisenberg operators

$$f^\alpha_{j\nu\sigma}(t)=e^{iHt}f^\alpha_{j\nu\sigma}e^{-iHt},\quad f^\alpha_{j\nu\sigma}(0)=f^\alpha_{j\nu\sigma}\ , \tag{6a}$$

etc., and the grand canonical average, $\langle\cdots\rangle$, is defined in the usual way

$$\langle\cdots\rangle=\text{Tr}e^{-\beta H}(\cdots)/\text{Tr}e^{-\beta H},\quad \beta^{-1}=k_BT\ , \tag{6b}$$

where T is the temperature. To solve for these Green's functions we introduce the projection operator $P^2=P$ as follows:

$$PX=\sum_{j'',\nu'',\alpha'',\sigma''}f^{\alpha''\dagger}_{j''\nu''\sigma''}\langle[f^{\alpha''}_{j''\nu''\sigma''},X]_+\rangle/\langle n^{\alpha''}_{j''\nu'',-\sigma''}\rangle\ , \tag{7a}$$

which has the property that, for all j,ν,α,σ,

$$Pf^{\alpha\dagger}_{j\nu\sigma}=f^{\alpha\dagger}_{j\nu\sigma},\quad (1-P)f^{\alpha\dagger}_{j\nu\sigma}=0\ . \tag{7b}$$

Since the projections defined in Eq. (7) involve the averages, $\langle n^{\alpha''}_{j''\nu''-\sigma''}\rangle$, it is convenient to write the equations of motion for the rescaled Green's functions defined as

$$\tilde G^{\alpha\alpha'}_{j\nu;j'\nu'\sigma}(t)=(\langle n^\alpha_{j\nu,-\sigma}\rangle\langle n^{\alpha'}_{j'\nu',-\sigma}\rangle)^{-1/2}G^{\alpha\alpha'}_{j\nu;j'\nu'\sigma}(t)\ , \tag{8a}$$

where, by construction,

$$i\tilde G^{\alpha\alpha'}_{j\nu;j'\nu'\sigma}(t=0)=\delta_{jj'}\delta_{\nu\nu'}\delta_{\alpha\alpha'}\ . \tag{8b}$$

This will yield equations of motion for the Green's functions with a Hermitian dynamical matrix. For arbitrary function A, its Laplace and spatial transforms are defined by

$$\begin{aligned} &A_{j\nu;j'\nu'}(\bar\omega)=\int_0^\infty dt\,e^{i\bar\omega t}A_{j\nu;j'\nu'}(t)\ ,\\ &\bar\omega=\omega+i0^+\ , \end{aligned} \tag{9a}$$

and

$$A_{jv;j'v'}=\frac{1}{N}\sum_{k} e^{ik(j-j')}A_{kvv'} , \tag{9b}$$

where N is the number of unit cells.

Using Eqs. (5)–(9) it is found that the exact equations of motion for the momentum and frequency dependent $\tilde{G}^{\alpha\alpha'}_{kvv'\sigma}(\bar{\omega})$'s are (the detailed derivation is given in the Appendix):

$$\sum_{\alpha''v''}\{\bar{\omega}\delta_{vv''}\delta_{\alpha\alpha''}-E^{\alpha\alpha''}_{kvv''\sigma}(\bar{\omega})\}\tilde{G}^{\alpha''\alpha'}_{kv''v'\sigma}(\bar{\omega})=\delta_{vv'}\delta_{\alpha\alpha'} , \tag{10a}$$

where the Hermitian energy matrix is defined by

$$E^{\alpha\alpha''}_{kvv''\sigma}(\bar{\omega})=\delta_{vv''}\delta_{\alpha\alpha''}\varepsilon^{\alpha}_{v}+t_{kvv''}(\langle n^{\alpha}_{v,-\sigma}\rangle\langle n^{\alpha''}_{v'',-\sigma}\rangle)^{1/2} +\alpha\alpha''[\Delta_{kvv''\sigma}+M_{kvv''\sigma}(\bar{\omega})] \times(\langle n^{\alpha}_{v,-\sigma}\rangle\langle n^{\alpha''}_{v'',-\sigma}\rangle)^{-1/2} \tag{10b}$$

and we have assumed that the "n" averages are independent of the unit cell. In Eq. (10b),

$$\varepsilon^{\alpha}_{v}=\varepsilon_{v}+U_{vv}\delta_{\alpha,+} . \tag{11}$$

The static mean-field corrections $\Delta_{kvv''\sigma}$ are the spatial transforms of

$$\Delta_{jv;j''v''\sigma}=\langle[f^{-}_{jv\sigma},L_{t}f^{-\dagger}_{j''v''\sigma}]_{+}\rangle -t_{jv;j''v''}\langle n^{-}_{v,-\sigma}\rangle\langle n^{-}_{v'',-\sigma}\rangle , \tag{12}$$

where L is the Liouville operator defined by $L=[H,\ ]_{-}$. L_t is defined as the commutator with respect to only that part of H of Eq. (3) which is proportional to the $\{t_{jv;j''v''}\}$'s. Finally, the dynamic memory functions, $M_{kvv''\sigma}(\bar{\omega})$, are the Laplace and spatial transforms of

$$M_{jv;j''v''\sigma}(t) =-i\langle[f^{-}_{jv\sigma},Le^{-it(1-P)L}(1-P)Lf^{-\dagger}_{j''v''\sigma}]_{+}\rangle . \tag{13}$$

In the energy matrix of Eq. (10b), if the $\Delta_{kvv''\sigma}$'s and $M_{kvv''\sigma}(\bar{\omega})$'s are to zero, one gets the Hubbard-I solution. Notice that the Hubbard-I solution misses these static and dynamic terms due to the naive truncation in the original Hubbard paper which essentially treats the "f" operators as if they were pure fermions. The complicated statistics of the $f^{\alpha}_{jv\sigma}$'s are automatically handled correctly when one truncates the equations of motion by using the projection operator given in Eq. (7), leading to the solutions given in Eq. (10). Finally, the projection-operator mean-field solution is that generated by setting all the memory functions $M_{kvv''\sigma}(\bar{\omega})$ to zero in Eq. (10), so that the energies in Eq. (10b) are independent of $\bar{\omega}$:

$$E^{\alpha\alpha''}_{kvv''\sigma}(\bar{\omega})=E^{\alpha\alpha''}_{kvv''\sigma} . \tag{14}$$

In this paper we will focus only on the mean-field results. Self-energy effects will be included elsewhere.

III. MEAN-FIELD RESULTS

We have used the projection-operator-based mean-field formalism presented in the last section to calculate various physical properties of the CuO_2 lattice and made comparisons between these results and those of quantum Monte Carlo simulations and other MF theories. In all figures shown here, the notations MC, POMF, and SBMF are used to represent the data points of the Monte Carlo simulation, the projection-operator mean-field calculations, and the four-boson mean-field theory. We set $U_{dp}=0$ throughout our calculations. Unless otherwise specified, the LDA parameters listed in Eq. (2) are used. $\beta=1/T$ is the inverse of temperature.

In Fig. 1, the Cu- and O-site occupation numbers versus band filling $\langle n\rangle=\langle n_{Cu}\rangle+2\langle n_{O}\rangle$ are shown. In the hole picture, $\langle n\rangle=1$ is the half-filled case. The parameters used in Fig. 1(a) are $t_{dp}=1$, $U_{dd}=6$, $\varepsilon=\varepsilon_p-\varepsilon_d=2$, $t_{pp}=U_{pp}=0$, and $\beta=8$ where MC results are available, and there is an excellent agreement between the POMF and MC results. At half-filling, the hole occupation on the Cu site is much larger than that on the O

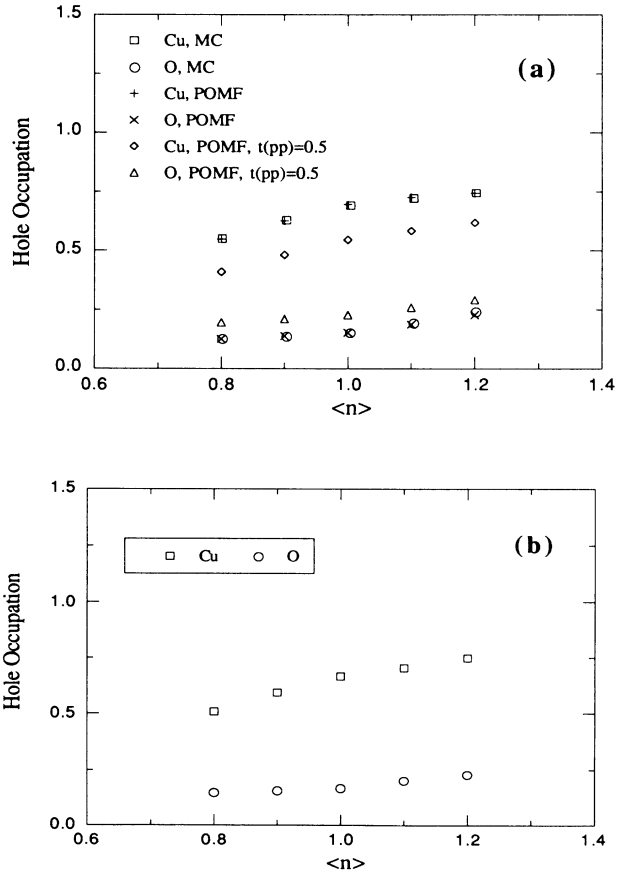

FIG. 1. The hole occupation numbers on the Cu site $\langle n_{Cu}\rangle$ and O site $\langle n_{O}\rangle$ vs band filling $\langle n\rangle=\langle n_{Cu}\rangle+2\langle n_{O}\rangle$. (a) Both of the Monte Carlo (Ref. 10) and the projection-operator mean-field results for $t_{dp}=1$, $U_{dd}=6$, $\varepsilon=2$, $t_{pp}=U_{pp}=0$, and $\beta=8$ are shown. Symbols $\Diamond$ and $\triangle$ are the data points for $\langle n_{Cu}\rangle$ and $\langle n_{O}\rangle$ with $t_{pp}=0.5$. (b) $\langle n_{Cu}\rangle$ and $\langle n_{O}\rangle$ vs $\langle n\rangle$ using the LDA parameters listed in Eq. (2).

site because of the low-lying singly occupied Cu d state. When the hole doping $\delta = \langle n \rangle - 1$ gets larger, it is seen that $\langle n_{Cu} \rangle$ shows little increase and most of the doped holes go to the O site. The opposite happens when there is electron doping ($\delta < 0$). This same observation can be made if LDA parameters are used and the result is plotted in Fig. 1(b) for $\beta = 10$.

To examine the effect of t_{pp}, we also show the POMF data in Fig. 1(a) for $t_{pp} = 0.5$. Due to the hopping of p electrons, thus the broadening of the O p band, there is a greater portion of p states mixed into the low-lying Cu d states, resulting in a larger $\langle n_O \rangle$ and smaller $\langle n_{Cu} \rangle$ comparing with $t_{pp} = 0$ in the half-filled case. With hole doping, the increase in $\langle n_O \rangle$ is not as rapid as when $t_{pp} = 0$, nonetheless, most of the doped holes still go to the O site.

In Fig. 2, the squared local moment $\langle m_z^2 \rangle = \langle (n_\uparrow - n_\downarrow)^2 \rangle$ on the Cu site versus U_{dd} [Fig. 2(a)] and versus ε [Fig. 2(b)] at half-filling is shown. To be able to compare with MC results, parameters $t_{dp} = 1$, $t_{pp} = 0$, $\varepsilon = 2U_{dd}/3$, $U_{pp} = 0$, and $\beta = 10$ are used in Fig. 2(a), $U_{dd} = 6$ and $\beta = 3$ in Fig. 2(b). Similar to the single-band Hubbard case, there is no antiferromagnetic solution in a certain parameter range within POMF. For parameters where an AF ground state can be found, POMF results of the Cu-squared local moment agree very well with those of MC simulations. For fixed t_{dp}, it is seen that U_{dd} tends to localize the spin on the Cu site. With a nonzero t_{pp}, the hole occupation on the Cu site becomes smaller, and Cu $\langle m_z^2 \rangle$ is suppressed. This is seen in Fig. 2(a) where the result for $t_{pp} = 0.5$ is plotted. This suppression of $\langle m_z^2 \rangle$ is more severe in the charge-transfer limit, as discussed elsewhere.[16]

To gain a better understanding of the physical properties presented above and in another paper,[16] we now concentrate on the density of states of the three-band CuO_2 lattice model with proper LDA parameters. Figure 3 shows Cu, O, and total density of states for the paramagnetic (PM) state and Fig. 4 shows the AF state in the half-filled case, with parameters listed in Eq. (2) and $\beta = 10$. In the PM state, the calculation clearly shows the three-band structure, with a mostly O p-state band in between the two bands dominated by singly occupied and doubly occupied Cu d states. For $\langle n \rangle = 1$, the Fermi energy (set to zero in figures and also indicated by the verti-

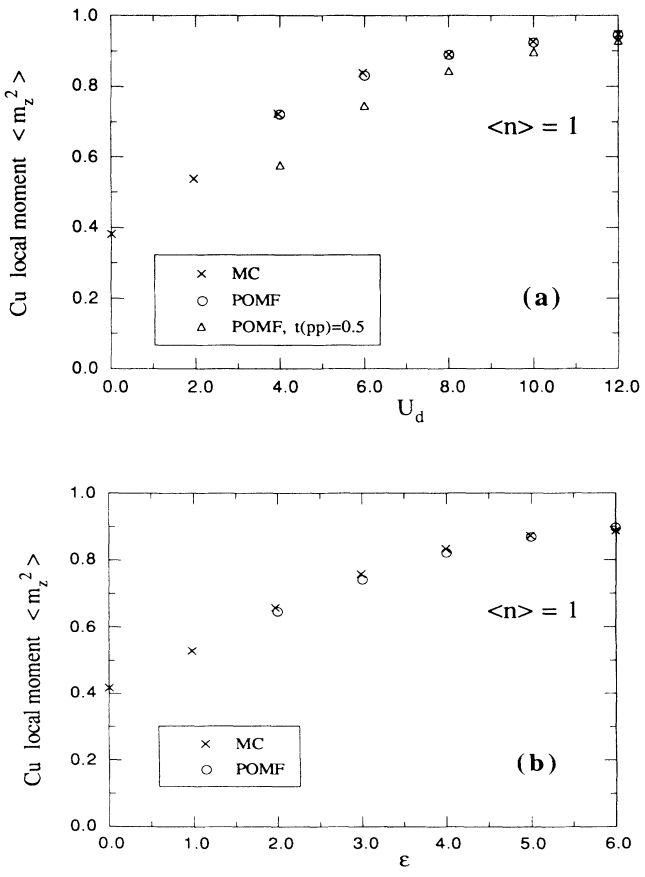

FIG. 2. The squared local moment on the Cu site $\langle m_z^2 \rangle = \langle (n_\uparrow - n_\downarrow)^2 \rangle$ vs U_{dd} [in (a)] and vs ε [in (b)]. $t_{dp} = 1$, $t_{pp} = 0$, $U_{pp} = 0$. In (a) $\varepsilon = 2U_{dd}/3$, $\beta = 10$. In (b) $U_{dd} = 6$, $\beta = 3$. The $\triangle$ symbol in (a) are the data points for $t_{pp} = 0.5$ from the POMF calculation. The Monte Carlo result is from Ref. 10.

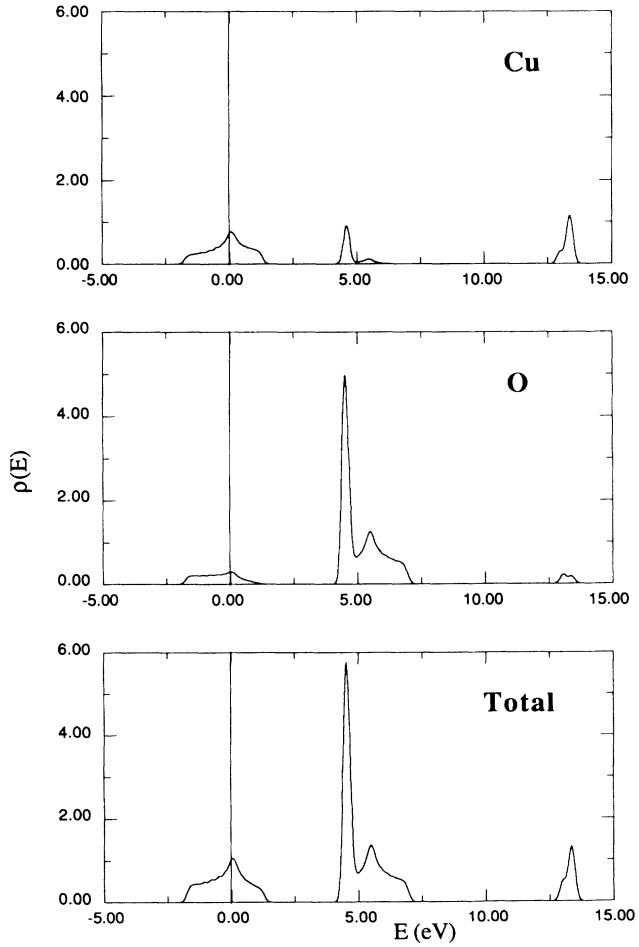

FIG. 3. The Cu, O, and total density of states for the paramagnetic half-filled system. The LDA parameters are used along with $\beta = 10$. The Fermi energy is set to be zero and marked by a vertical line.

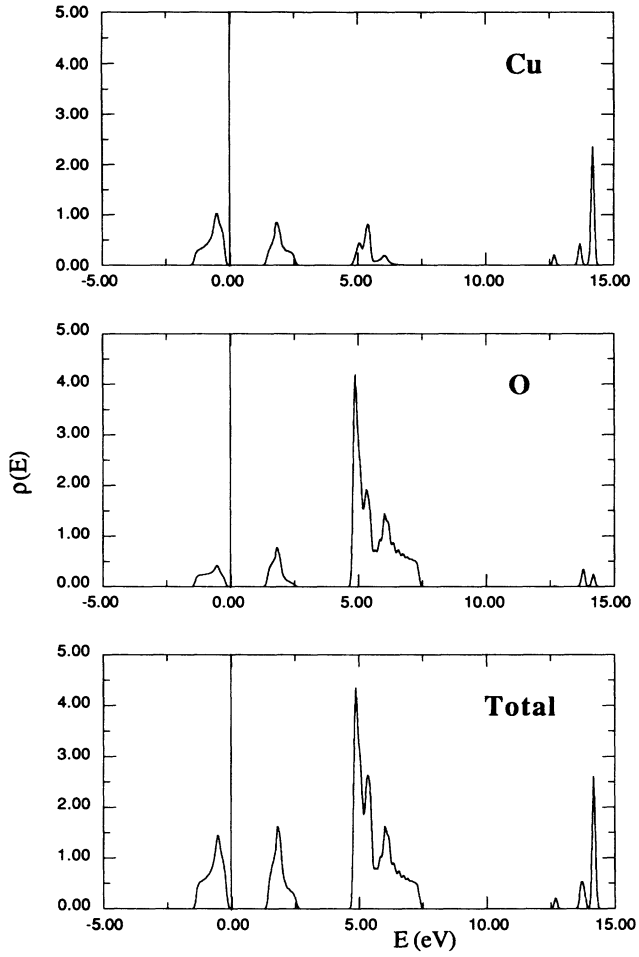

FIG. 4. The density of states for the antiferromagnetic half-filled system. Parameters are the same as those used in Fig. 3.

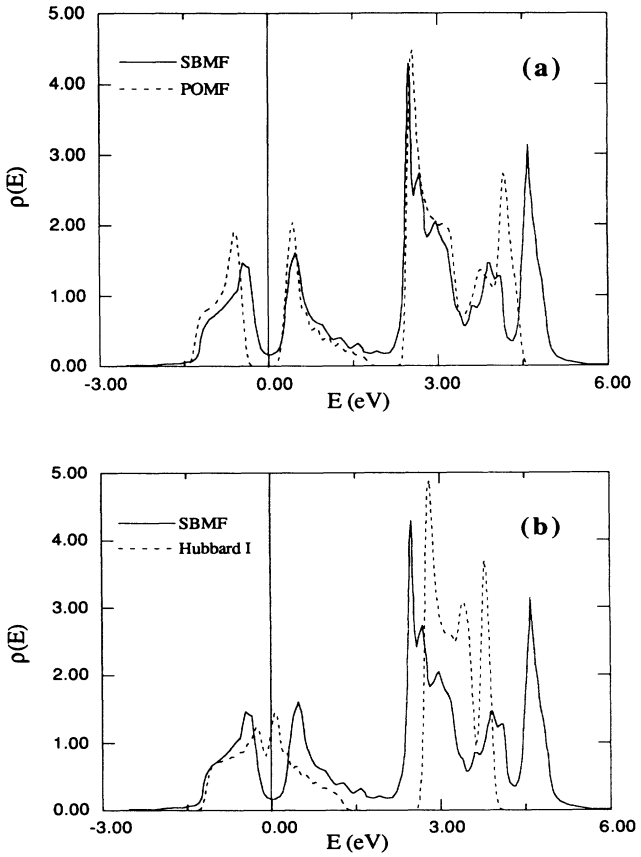

FIG. 5. The comparison of density of states obtained from the four-boson theory (SBMF, Ref. 12), the projection-operator mean-field (POMF) calculation and the Hubbard-I approximation. At half-filling $\langle n \rangle = 1$, with $U_{dd} = 6$ eV, $\varepsilon = 1.5$ eV, $t_{dp} = 1.085$ eV, $t_{pp} = 0.2$ eV, and $U_{pp} = 0$. The high-energy structures in the POMF and Hubbard-I results are not shown in the graph. (a) The DOS from SBMF and POMF are very similar. $\beta = 10$ in POMF. (b) The DOS from the Hubbard-I approximation is distinctively different from that from SBMF. $\beta = 40$ is used in the Hubbard-I calculation in order to get the AF solution.

cal line) lies in the middle of the d band. In the AF state, this low-lying band splits, leaving the Fermi level in the gap. Since the AF state has a lower energy, the undoped system is an insulator.

As discussed in the last section, the difference between Hubbard I and POMF is the static energy shift Δ. For the single-band Hubbard model, the POMF calculation shows a systematic improvement[14] over that of Hubbard I. In Fig. 5, we make a comparison between the results of total DOS for the AF ground state of undoped system ($\langle n \rangle = 1$) from POMF, Hubbard I, and the four-boson theory (SBMF).[12] The parameters used are the same as those in Ref. 12, which are $U_{dd} = 6$ eV, $\varepsilon = 1.5$ eV, $t_{dp} = 1.085$ eV, $t_{pp} = 0.2$ eV, and $U_{pp} = 0$. All Fermi levels (vertical lines) are set to zero in the figure. It is seen that the DOS from POMF and SBMF are similar [Fig. 5(a)], except that in SBMF there is no high-energy Hubbard-like band for the doubly occupied Cu d states which always exists in the POMF and the Hubbard-I approximation (not shown in Fig. 5). Both the POMF and SBMF results indicate an insulating system, with Fermi energy inside the AF band gap. But the DOS results obtained from the Hubbard-I calculation show a rather different structure around the Fermi energy, yielding an unphysical metallic ground state at half-filling. Thus, as in the single-band Hubbard model case, the static energy shift Δ used in the POMF is important for getting the correct physical properties.

In order to examine the effect of doping on the magnetic order, the staggered magnetization on the Cu site $\langle m_z \rangle = |\langle n_\uparrow - n_\downarrow \rangle|$ versus band filling $\langle n \rangle$ with LDA parameters and $\beta = 10$ is calculated, and the results are shown in Fig. 6. Without doping ($\delta = 0$), $\langle m_z \rangle$ has its maximum value. As the doping (hole or electron) gets larger and larger, the staggered magnetization becomes smaller and smaller as expected, and eventually vanishes, yielding a paramagnetic ground state. We point out that we considered only simple AF order in our calculations and have not addressed the stability of the various spiral phases which occur in the limit of small doping due to the strong coupling to the spin background.[17] We feel that this MF calculation is inadequate in the small doping regime and thus have not focused on this region.

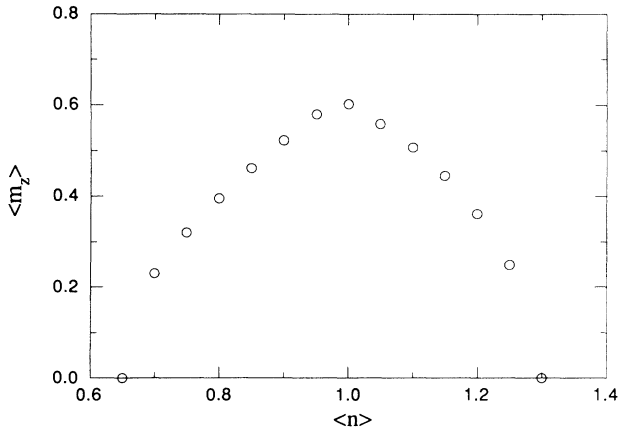

FIG. 6. The staggered magnetic moment $\langle m_z \rangle = |\langle n_\uparrow - n_\downarrow \rangle|$ on the Cu site vs band filling $\langle n \rangle$. The LDA parameters are used with $\beta = 10$. Note that $\langle n \rangle > 1$ corresponds to hole doping, and $\langle n \rangle < 1$ corresponds to electron doping.

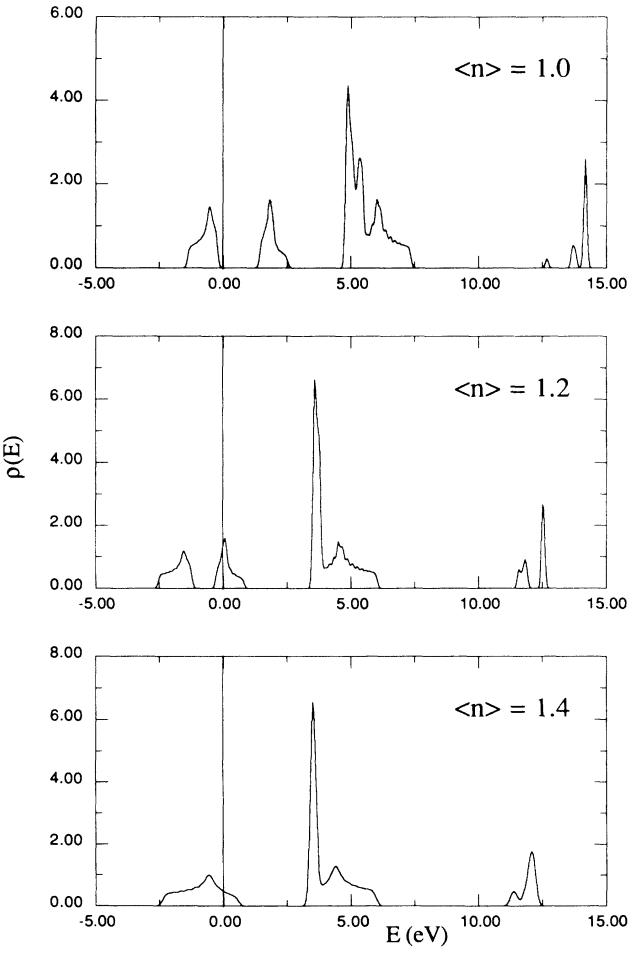

FIG. 7. The total density of states for band fillings $\langle n \rangle = 1.0$, 1.2, and 1.4. Parameters are the same as those used in Fig. 6. The Fermi energy is set to zero (vertical line). The ground states for $\langle n \rangle = 1.0$ and 1.2 are AF while for $\langle n \rangle = 1.4$ the state is PM.

Also, we did not consider the question of phase separation since we did not do a detailed study of the role of U_{dp}.

The role of doping in inducing a transition from the AF ground state at $\delta = 0$ to the PM ground state at finite doping can be better understood by examining the density of states of the system as a function of δ. The total DOS for $\delta = 0$, 0.2, and 0.4 is plotted in Fig. 7 with the same parameters as those used in Fig. 6. As we have shown earlier, the system is an insulator with Fermi level lies in the AF band gap for $\delta = 0$. Even at 20% hole doping, the ground state is still AF (Fig. 6) but the Fermi level has moved into the upper singly occupied Cu AF band and the AF band gap is smaller. As δ gets larger this gap eventually vanishes and the system becomes PM. This is seen for the case $\delta = 0.4$.

In Fig. 5, a distinct difference between the total DOS obtained from the POMF and the Hubbard-I scheme is shown for the AF ground state. For the PM ground state, this difference is shown in Fig. 8, where $\langle n \rangle = 1.5$, temperature $T = 100$ K ($\beta = 10^{-2}$). The Fermi level is inside the low-lying d band for the POMF, but for the Hubbard-I, it lies inside the p band. Also compared to the DOS of POMF, the Hubbard-I calculation yields a

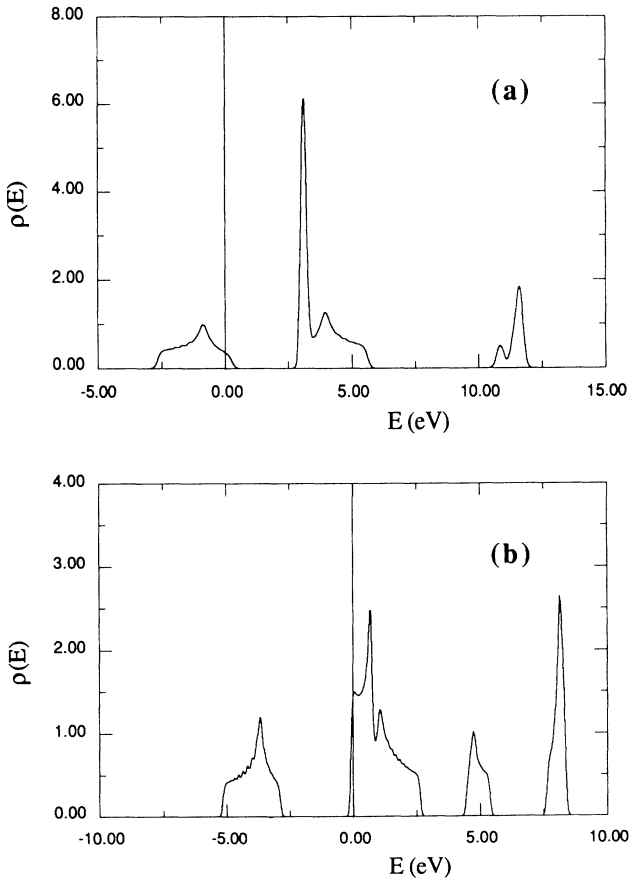

FIG. 8. The total density of states obtained from (a) the POMF and (b) the Hubbard-I calculations for $\langle n \rangle = 1.5$. LDA parameters are used with temperature $T = 100$ K ($\beta = 10^{-2}$). The ground state is PM in this case.

separate p-state dominated band around 5 eV. It is interesting to see that even though the Coulomb repulsion U_{dp} between electrons on Cu and O sites is not incorporated in this current calculation, the resulting total DOS in Fig. 8(b) is similar to those in Figs. 4(b) and 8(b) of Ref. 13 in which all parameters used are the same as those in Fig. 8 except $U_{dp}=1.2$ eV. This implies that, even with certain restrictions,[13] the Hubbard-I approximation may yield a qualitatively different position of Fermi level in the DOS result from the POMF and SBMF calculations.

IV. CONCLUSION

We have applied our projection-operator-based mean-field formalism to the three-band Hubbard model for a wide range of input parameters. Where quantum Monte Carlo results are available (i.e., for $t_{pp}=0$), our calculations for hole occupations on Cu and O sites and for magnetic moments compare remarkably well with MC results. The hole density of states results have been presented for both antiferromagnetic and paramagnetic states using the LDA energy parameters. An antiferromagnetic ground state is obtained for a half-filled system, with the Fermi level lying in the AF band gap. It is observed that this DOS result resembles that from the slave-boson theory, but is distinctively different from the Hubbard-I approximation. With hole doping, the AF band gap gradually disappears, and the Fermi level moves into the energy band dominated by O p states, so that the doped holes tend to go to O sites.

Since our formalism compares well with available MC results, we feel confident about our results in the region of finite t_{pp} where no MC results are available. We show that, by allowing electrons to hop between two neighboring O atoms, the energy band dominated by O p states is broadened, thus the number of holes on the O sites increase, and the magnetic moments on the Cu sites are suppressed. Our POMF formalism requires fewer numbers of coupled equations to be solved self-consistently and we are able to investigate the effects of a large set of energy parameters systematically without great difficulty.

ACKNOWLEDGMENTS

We would like to thank S. P. Bowen and D. D. Koelling for useful discussions, and D. J. Scalapino for supplying the Monte Carlo data. This work is supported by the U.S. Department of Energy at Argonne National Laboratory, Basic Energy Sciences-Materials Sciences, under Contract No. W-31-109-Eng-38, and by the U.S. Department of Energy at Iowa State University under Contract No. W-74005-Eng-82, and by the Florida State University Supercomputer Computations Research Institute which is partially funded by the U.S. Department of Energy under Contract No. DE-FC05-85ER250000.

APPENDIX: DERIVATION OF THE EQUATIONS OF MOTION FOR THE GREEN'S FUNCTIONS

In this appendix we derive the exact set of equations for the Green's functions given in Eq. (10). In terms of the Liouville operator $LA=[H,A]_-$, the Heisenberg time dependence of an arbitrary operator A can be written as

$$A(t)=e^{iHt}Ae^{-iHt}=e^{iLt}A, \quad A(0)=A \ . \tag{A1}$$

Then the retarded Green's functions $G^{\alpha\alpha'}_{jv;j'v'\sigma}(t)$ of Eq. (5) become

$$G^{\alpha\alpha'}_{jv;j'v'\sigma}(t)=-i\langle[f^{\alpha}_{jv\sigma},f^{\alpha'\dagger}_{j'v'\sigma}(-t)]_+\rangle \ , \tag{A2}$$

using the identity

$$\langle[A,L^nB]_+\rangle=\langle[(-L)^nA,B]_+\rangle, \quad n=0,1,2,\ldots \ . \tag{A3}$$

From Eqs. (A1) and (A2), the equation of motion is

$$\begin{aligned} i\frac{\partial G^{\alpha\alpha'}_{jv;j'v'\sigma}(t)}{\partial t}&=-i\langle[f^{\alpha}_{jv\sigma},Lf^{\alpha'\dagger}_{j'v'\sigma}(-t)]_+\rangle \\ &=-i\langle[f^{\alpha}_{jv\sigma},L\{P+(1-P)\}f^{\alpha'\dagger}_{j'v'\sigma}(-t)]_+\rangle \end{aligned} \tag{A4}$$

for any operator P. In this case the projection operator defined in Eq. (7) is used for P. Now the basic idea of the projection scheme is to write the term $P(f^{\alpha'}_{j'v'\sigma})^+(-t)$ in terms of the original Green's function at the same time t resulting in static (mean-field) contributions. The remaining term, $(1-P)(f^{\alpha'}_{j'v'\sigma})^+(-t)$, which is orthogonal to this static term (since $P^2=P$), is then written in terms of an integral of the original Green's function over all earlier times τ such that $\tau<t$ yielding the dynamic (self-energy) terms termed memory functions. This is done as follows: From Eqs. (A2) and (7) it is easily seen that

$$Pf^{\alpha'\dagger}_{j'v'\sigma}(-t)=i\sum_{j'',v'',\alpha''}[f^{\alpha''\dagger}_{j''v''\sigma}/\langle n^{\alpha''}_{j''v'',-\sigma}\rangle]G^{\alpha''\alpha'}_{j''v'';j'v'\sigma}(t) \ . \tag{A5}$$

Now, for any Heisenberg operator, $A(-t)$, there is the operator identity

$$(1-P)A(-t)=e^{-it(1-P)L}(1-P)A(0)-i\int_0^t d\tau\, e^{-i(t-\tau)(1-P)L}(1-P)LPA(-\tau) \ . \tag{A6}$$

Obviously this expression is correct at $t=0$. To verify that it is valid for all times t, simply differentiate both sides of this expression with respect to time and show that they are equal. By use of Eqs. (A2), (7), and (A6), one finds immediately

$$(1-P)f^{\alpha'\dagger}_{j'v'\sigma}(-t)=\sum_{j'',v'',\alpha''}\int_0^t d\tau\{e^{-i(t-\tau)(1-P)L}(1-P)Lf^{\alpha''\dagger}_{j''v''\sigma}/\langle n^{\alpha''}_{j''v'',-\sigma}\rangle\}G^{\alpha''\alpha'}_{j''v'';j'v'\sigma}(\tau) \ . \tag{A7}$$

Now use of Eqs. (A5) and (A7) in (A3) gives the exact equations of motion for the Green's functions which can be writ-

ten as follows:

$$i\frac{\partial G^{\alpha\alpha'}_{jv;j'v'\sigma}(t)}{\partial t}=\sum_{j'',v'',\alpha''}\{\Omega^{\alpha\alpha''}_{jv;j''v''\sigma}/\langle n^{\alpha''}_{j''v'',-\sigma}\rangle\}G^{\alpha''\alpha'}_{j''v'';j'v'\sigma}(t)+\sum_{j'',v'',\alpha''}\int_0^t d\tau\{M^{\alpha\alpha''}_{jv;j''v''\sigma}(t-\tau)/\langle n^{\alpha''}_{j''v'',-\sigma}\rangle\}G^{\alpha''\alpha'}_{j''v'';j'v'\sigma}(\tau)\ , \tag{A8}$$

where the state (mean-field) terms are defined by

$$\Omega^{\alpha\alpha''}_{jv;j''v''\sigma}=\langle[f^{\alpha}_{jv\sigma},Lf^{\alpha''\dagger}_{j''v''\sigma}]_+\rangle \tag{A9}$$

and the memory functions are

$$M^{\alpha\alpha''}_{jv;j''v''\sigma}(t)=-i\langle[f^{\alpha}_{jv\sigma},Le^{-it(1-P)L}(1-P)Lf^{\alpha''\dagger}_{j''v''\sigma}]_+\rangle\ . \tag{A10}$$

The functions, defined in Eqs. (A9) and (A10) for the various α,α'' combinations, can be simplified as follows: From Eqs. (3) and (4) we find

$$Lf^{\alpha\dagger}_{jv\sigma}=\varepsilon^{\alpha}_{v}f^{\alpha\dagger}_{jv\sigma}+\sum_{j',v'}t_{jv;j'v'}\{n^{\alpha}_{jv,-\sigma}c^{\dagger}_{j'v'\sigma}+(\delta_{\alpha,+}-\delta_{\alpha,-})[c^{\dagger}_{j'v}c_{jv,-\sigma}-c^{\dagger}_{jv,-\sigma}c_{j'v',-\sigma}]c^{\dagger}_{jv\sigma}\}\ , \tag{A11a}$$

where the energy

$$\varepsilon^{\alpha}_{v}=\varepsilon_{v}+U_{vv}\delta_{\alpha,+}\ . \tag{A11b}$$

From Eqs. (7) and (A11) one finds the following identities:

$$\sum_{\alpha}(1-P)Lf^{\alpha\dagger}_{jv\sigma}=(1-P)Lc^{\dagger}_{jv\sigma}=0 \tag{A12a}$$

and

$$\langle[-Lc_{jv\sigma},(1-P)Z]_+\rangle=0 \tag{A12b}$$

for any operator Z. Use of Eq. (A12) in (A10) gives immediately

$$\sum_{\alpha}M^{\alpha\alpha''}_{jv;j''v''\sigma}(t)=0,\quad\sum_{\alpha''}M^{\alpha\alpha''}_{jv;j''v''\sigma}(t)=0\ . \tag{A13}$$

Thus, from Eq. (A13),

$$M^{\alpha\alpha''}_{jv;j''v''\sigma}(t)=\alpha\alpha''M_{jv;j''v''\sigma}(t)\ , \tag{A14a}$$

where

$$M_{jv;j''v''\sigma}(t)=M^{--}_{jv;j''v''\sigma}(t)\ . \tag{A14b}$$

A similar analysis can be done for the "mean-field" terms $\Omega^{\alpha\alpha''}_{jv;j''v''\sigma}$ defined in Eq. (A9). From Eqs. (A3) and (A11),

$$\begin{aligned}\langle[f^{\alpha}_{jv\sigma},Lf^{\alpha''\dagger}_{j''v''\sigma}]_+\rangle&=\langle[-Lf^{\alpha}_{jv\sigma},f^{\alpha''\dagger}_{j''v''\sigma}]_+\rangle\\&=\delta_{jj''}\delta_{vv''}\delta_{\alpha\alpha''}\varepsilon^{\alpha}_{v}\langle n^{\alpha}_{jv,-\sigma}\rangle\\&\quad+t_{jv;j''v''}\langle n^{\alpha}_{jv,-\sigma}\rangle\langle n^{\alpha''}_{j''v'',-\sigma}\rangle\\&\quad+\Delta^{\alpha\alpha''}_{jv;j''v''\sigma}\ ,\end{aligned} \tag{A15a}$$

where $\Delta^{\alpha\alpha''}_{jv;j''v''\sigma}$ is defined as

$$\begin{aligned}\Delta^{\alpha\alpha''}_{jv;j''v''\sigma}&=\langle[f^{\alpha}_{jv\sigma},L_tf^{\alpha''\dagger}_{j''v''\sigma}]_+\rangle\\&\quad-t_{jv;j''v''}\langle n^{\alpha}_{jv,-\sigma}\rangle\langle n^{\alpha''}_{j''v'',-\sigma}\rangle\\&=\langle[-L_tf^{\alpha}_{jv\sigma},f^{\alpha''\dagger}_{j''v''\sigma}]_+\rangle\\&\quad-t_{jv;j''v''}\langle n^{\alpha}_{jv,-\sigma}\rangle\langle n^{\alpha''}_{j''v'',-\sigma}\rangle\end{aligned} \tag{A15b}$$

in which L_t is defined as the commutator with respect to that part of H defined in Eq. (3) proportional to the $\{t_{jv;j'v'}\}$'s. Use of Eq. (A11) in (A15b) gives, by construction,

$$\sum_{\alpha}\Delta^{\alpha\alpha''}_{jv;j''v''\sigma}=0,\quad\sum_{\alpha''}\Delta^{\alpha\alpha''}_{jv;j''v''\sigma}=0\ . \tag{A16}$$

Thus, from Eq. (A16) one gets, just as in Eq. (A14),

$$\Delta^{\alpha\alpha''}_{jv;j''v''\sigma}=\alpha\alpha''\Delta_{jv;j''v''\sigma}\ , \tag{A17a}$$

where

$$\Delta_{jv;j''v''\sigma}=\Delta^{--}_{jv;j''v''\sigma}\ , \tag{A17b}$$

Using the results of Eqs. (A14) and (A17) in (A8),

$$\begin{aligned}\left[i\frac{\partial}{\partial t}-\varepsilon^{\alpha}_{v}\right]G^{\alpha\alpha'}_{jv;j'v'\sigma}(t)&=\sum_{j'',v'',\alpha''}t_{jv;j''v''}\langle n^{\alpha}_{jv,-\sigma}\rangle G^{\alpha''\alpha'}_{j''v'',j'v'\sigma}(t)+\sum_{j'',v'',\alpha''}\alpha\alpha''[\Delta_{jv;j''v''\sigma}/\langle n^{\alpha''}_{j''v'',-\sigma}\rangle]G^{\alpha''\alpha'}_{j''v'';j'v'\sigma}(t)\\&\quad+\sum_{j'',v'',\alpha''}\int_0^t d\tau\{\alpha\alpha''M_{jv;j''v''\sigma}(t-\tau)/\langle n^{\alpha''}_{j''v'',-\sigma}\rangle\}G^{\alpha''\alpha'}_{j''v'';j'v'\sigma}(\tau)\ .\end{aligned} \tag{A18}$$

Since the projections defined in Eq. (7) involve the averages $\langle n^{\alpha''}_{j''v''-\sigma''}\rangle$ in the denominator, it is convenient to write the equations of motion for the rescaled Green's functions defined as follows:

$$\tilde{G}^{\alpha\alpha'}_{jv;j'v'\sigma}(t)=(\langle n^{\alpha}_{jv,-\sigma}\rangle\langle n^{\alpha'}_{j'v',-\sigma}\rangle)^{-1/2}G^{\alpha\alpha'}_{jv;j'v'\sigma}(t)\ , \tag{A19a}$$

where, by construction,

$$i\tilde{G}^{\alpha\alpha'}_{jv;j'v'\sigma}(t=0)=\delta_{jj'}\delta_{vv'}\delta_{\alpha\alpha'} . \tag{A19b}$$

One can then rewrite the Green's-function equations of motion given in Eq. (A18) in terms of $\tilde{G}^{\alpha\alpha'}_{jv;j'v'\sigma}(t)$. Using Eqs. (A18) and (A19),

$$\left[i\frac{\partial}{\partial t}-\varepsilon^{\alpha}_{v}\right]\tilde{G}^{\alpha\alpha'}_{jv;j'v'\sigma}(t)=\sum_{j'',v'',\alpha''} t_{jv;j''v''}(\langle n^{\alpha}_{jv,-\sigma}\rangle\langle n^{\alpha''}_{j''v'',-\sigma}\rangle)^{1/2}\tilde{G}^{\alpha''\alpha'}_{j''v'';j'v'\sigma}(t)$$
$$+\sum_{j'',v'',\alpha''}\alpha\alpha''\Delta_{jv;j''v''\sigma}(\langle n^{\alpha}_{jv,-\sigma}\rangle\langle n^{\alpha''}_{j''v'',-\sigma}\rangle)^{-1/2}\tilde{G}^{\alpha''\alpha'}_{j''v'';j'v'\sigma}(t)$$
$$+\sum_{j'',v'',\alpha''}\alpha\alpha''\int_0^t d\tau M_{jv;j''v''\sigma}(t-\tau)(\langle n^{\alpha}_{jv,-\sigma}\rangle\langle n^{\alpha''}_{j''v'',-\sigma}\rangle)^{-1/2}\tilde{G}^{\alpha''\alpha'}_{j''v'';j'v'\sigma}(\tau) . \tag{A20}$$

For arbitrary A, its Laplace and spatial transformations are

$$A_{jj'}(\bar{\omega})=\int_0^{\infty} dt\, e^{i\bar{\omega}t}A_{jj'}(t),\quad \bar{\omega}=\omega+i0^{+} , \tag{A21a}$$

and

$$A_{jj'}=\frac{1}{N}\sum_{k} e^{ik(j-j')}A_k . \tag{A21b}$$

Use of Eq. (A21) in (A20) gives

$$\sum_{\alpha''v''}\{\bar{\omega}\delta_{vv''}\delta_{\alpha\alpha''}-E^{\alpha\alpha''}_{kvv''\sigma}(\bar{\omega})\}\tilde{G}^{\alpha''\alpha'}_{kv''v'\sigma}(\bar{\omega})=\delta_{vv'}\delta_{\alpha\alpha'} , \tag{A22a}$$

where

$$E^{\alpha\alpha''}_{kvv''\sigma}(\bar{\omega})=\delta_{vv''}\delta_{\alpha\alpha''}\varepsilon^{\alpha}_{v}+t_{kvv''}(\langle n^{\alpha}_{v,-\sigma}\rangle\langle n^{\alpha''}_{v'',-\sigma}\rangle)^{1/2}$$
$$+\alpha\alpha''[\Delta_{kvv''\sigma}+M_{kvv''\sigma}(\bar{\omega})]$$
$$\times(\langle n^{\alpha}_{v,-\sigma}\rangle\langle n^{\alpha''}_{v'',-\sigma}\rangle)^{-1/2} . \tag{A22b}$$

It is now seen that the energy matrix is Hermitian. This completes the analysis.

[1] J. Hubbard, Proc. R. Soc. London, Ser. A **276**, 238 (1963).

[2] E. Dagotto, A. Moreo, and T. Barnes, Phys. Rev. B **40**, 6721 (1989); H. Q. Lin and J. E. Hirsch, *ibid.* **37**, 1864 (1988); J. Callaway, D. P. Chen, and Y. Zhang, *ibid.* **36**, 2084 (1987).

[3] A. Moreo, D. J. Scalapino, R. L. Sugar, S. R. White, and N. E. Bickers, Phys. Rev. B **41**, 2313 (1990); S. R. White *et al.*, *ibid.* **40**, 506 (1989); J. E. Hirsch, *ibid.* **31**, 4403 (1985).

[4] G. Geipel and W. Nolting, Phys. Rev. B **38**, 2608 (1988).

[5] E. G. Goryachev, E. V. Kuzmin, and S. G. Ovchinnikov, J. Phys. C **15**, 1481 (1982).

[6] V. Yu. Yushankhai, N. M. Plakida, and P. Kalinay, Physica C **174**, 401 (1991).

[7] G. Kotliar and A. E. Ruckenstein, Phys. Rev. Lett **57**, 1362 (1986).

[8] A. E. Ruckenstein, P. J. Hirschfeld, and J. Appel, Phys. Rev. B **36**, 375 (1987); G. Kotliar *ibid.* **37**, 3664 (1988).

[9] V. J. Emery, Phys. Rev. Lett. **58**, 2794 (1987).

[10] R. T. Scalettar, D. J. Scalapino, R. L. Sugar, and S. R. White, Phys. Rev. B **44**, 770 (1991).

[11] G. Dopf, A. Muramatsu, and W. Hanke, Phys. Rev. B **41**, 9264 (1990).

[12] W. Zhang, M. Avignon, and K. H. Bennemann, Phys. Rev. B **42**, 10 192 (1990).

[13] P. Entel and J. Zielinski, Phys. Rev. B **42**, 307 (1990).

[14] Yu. Zhou, A. J. Fedro, S. P. Bowen, D. D. Koelling, T. C. Leung, B. N. Harmon, and S. K. Sinha, Phys. Rev. B **44**, 10 291 (1991).

[15] M. S. Hybertsen, E. B. Stechel, M. Schluter, and D. R. Jennison, Phys. Rev. B **41**, 11 068 (1990); A. K. McMahan, J. F. Annett, and R. M. Martin, *ibid.* **42**, 6268 (1990).

[16] A. J. Fedro, Y. Zhou, T. C. Leung, and B. N. Harmon, in *High Temperature Superconductivity: Physical Properties, Microscopics and Mechanism,* edited by J. Ashkenazi, S. E. Barnes, F. Zuo, G. C. Vezzoli, and B. M. Klein (Plenum, New York, 1991), pp. 37–44.

[17] Extensive work has been done on the magnetic properties near half-filling. See, e.g., M. Grilli and G. Kotliar, Phys. Rev. Lett. **64**, 1170 (1990); B. Shraiman and E. Siggia, *ibid.* **62**, 1564 (1989).